Chemical Science

ROYAL SOCIETY OF CHEMISTRY

EDGE ARTICLE

View Article Online
View Journal | View Issue

Check for updates

Cite this: *Chem. Sci.*, 2024, **15**, 17017

All publication charges for this article have been paid for by the Royal Society of Chemistry

Received 12th April 2024
Accepted 28th August 2024

DOI: 10.1039/d4sc02474e

rsc.li/chemical-science

Open Access Article. Published on 30 August 2024. Downloaded on 12/13/2025 10:22:42 AM. This article is licensed under a Creative Commons Attribution-NonCommercial 3.0 Unported Licence.

Acylhydrazone-based reversibly photoswitchable ion pair transporter with OFF–ON cotransport activity†

Sandip Chattopadhayay, ‡ Paras Wanjari ‡§ and Pinaki Talukdar *

The cellular membrane transport of physiologically important cations and anions is omnipresent and regulates different physiological functions. Whereas a notable number of cation–anion transporters are being developed to transport salts across the membrane, developing an artificial cation–anion symporter with stimulus-responsive activities is an immense obstacle. Herein, for the first time, we report reversibly photoswitchable acylhydrazone-based transporter **2** that has distinctive OFF–ON cation–anion co-transport abilities. The substituent was modified in **1a–1c** and **2**, to change the to-and-fro movement of the transporter to enhance the ion transport efficiency. Ion transport experiments across the lipid bilayer membrane demonstrate that **1a** has the highest transport activity among the series with irreversible photoisomerization properties, whereas **2** has a unique reversible photoisomerization property. A detailed transport study indicated that the *E*-conformer of compound **2** facilitates Na^+/Cl^- transport *via* the symport process by following the carrier mode of ion transport. ^{23}Na NMR and chloride selective electrode assays confirmed the OFF and ON state of ion transport of compound **2** with photoirradiation. An assembly of $[(\mathbf{2}_E)_2$ + NaCl] was subjected to geometry optimization to understand the responsible ion binding motif. Geometry optimization followed by the natural bond orbital analysis of $\mathbf{1a}_Z$ and $\mathbf{2}_Z$ demonstrated that $\mathbf{1a}_Z$ forms comparatively stronger intramolecular H-bonding than $\mathbf{2}_Z$, making it accessible for reversible photoisomerization.

1 Introduction

Appropriate concentrations of physiologically important ions (Na^+, K^+, Cl^-, *etc.*) are crucial for the functioning of different biological processes, including regulating cardiac and neuronal activity, systemic pH, salt and water homeostasis, and cell proliferation, differentiation, and apoptosis.[1–3] Structurally and functionally complex transmembrane cation–anion cotransporters (CACs)[4–6] are one of the classes of transmembrane proteins that mediate electroneutral transport of cations and anions across the cellular membrane according to the requirement of the cells. Dysfunction of these transmembrane proteins is linked to several pathologies that are generally termed channelopathies, which comprise a plethora of diverse diseases, including epilepsy, migraine, cardiac arrhythmia, asthma, cystic fibrosis, cancer, *etc.*[7–9] Hence, chemical modification of natural transmembrane proteins[10–12] or developing small molecule-based synthetic transporters[13–15] is a vintage strategy that is still intriguing for giving structural and functional information. Moreover, recent findings revealed that synthetic transporters have the potential for antibacterial[16–18] and anticancer[19–21] activities. Such an interesting outcome with the synthetic transporter motivated us to design new synthetic ion transporter systems that can translocate ions across the bilayer membrane. Over time, scientists have developed cation[22,23] and anion[24–26] transporters to mimic the structures and functions of natural ion transporters and their application in various biological contexts. In recent years, cation–anion transporters have also been developed to realize the more complex dual ion selectivity. Synthetic K^+–Cl^- and Na^+–Cl^- symporting carriers, based on the salt-binding macrobicycle, were first invented by Smith and coworkers.[27] Following this, Kyu-Sung Jeong,[28] Philip A. Gale,[29] Stefan Matile,[30] Yun-Bao Jiang,[31] and Nandita Madhavan[32] and coworkers have also developed synthetic symporter carriers that can transport cation–anion across the bilayer. Alongside, Madhavan and our group have also made an efficient effort to develop cation–anion symporter channels.[19,32,33] Despite the advances in cation–anion transport, the non-stimulus response of these systems is a major limitation for real-life applications.

Department of Chemistry, Indian Institute of Science Education and Research Pune, Dr Homi Bhabha Road, Pashan, Pune 411008, Maharashtra, India. E-mail: ptalukdar@iiserpune.ac.in

† Electronic supplementary information (ESI) available. See DOI: https://doi.org/10.1039/d4sc02474e

‡ Authors contributed equally.

§ Present address: Institut Europeen des Membranes, University of Montpellier, ENSCM-CNRS, UMR 5635 Place E. Bataillon CC047, 34095 Montpellier, France.

© 2024 The Author(s). Published by the Royal Society of Chemistry

Open Access Article. Published on 30 August 2024. Downloaded on 12/13/2025 10:22:42 AM. This article is licensed under a Creative Commons Attribution-NonCommercial 3.0 Unported Licence.

A variety of synthetic gated ion transporters that involve pH, enzymes, voltage, light, redox, ligands, *etc.*, as external stimuli are reported.[34–39] Among these, light is a suitable choice as an external stimulus due to its wide control at the molecular level with high spatiotemporal precision.[40] To this extent, various photoresponsive transmembrane transporters based on stilbene,[41,42] azobenzene,[43,44] *o*-nitrobenzyl,[45,46] and acyl hydrazone[47,48] have been reported in the literature. Although acyl hydrazone-based systems have both cationic and anionic sites, their usage as a photoresponsive cation–anion symporter is unprecedented. In 2017, Zhou *et al.* showed that an acyl hydrazone-based molecule could be utilized to photoregulate the ion channel formation with different wavelengths of UV light, thus regulating the cation transport.[49] Our group also made an appreciable attempt to make an acylhydrazone-based transmembrane carrier that can photocontrol the transport of anions across the lipid bilayer membrane.[47,48] But all of these systems either transport cations or anions. Moreover, the use of UV-B region (280 nm–320 nm) of light for the deactivation process or redox stimulus in the reactivation process makes it difficult to use in real-life biological applications. The sparsity of these acyl-hydrazone-based cation–anion transporters with reversible ON and OFF transport activity stimulates us to develop stimulus-responsive small molecule-based cation–anion synthetic transporters.

Herein, we have reported a series of acylhydrazone-based cation–anion transporters **1a–1c** and **2** whose transport activity can be controlled spatiotemporally with the help of a specific wavelength of electromagnetic radiations to achieve both ON and OFF state of ion transport (Fig. 1). A series of derivatives were synthesized to modulate the ion transport activity by altering its insertion efficiency into the bilayer. Compound **1a** is supposed to show its higher transport activity among the congeners **1a–1c** due to its optimum logP value. In investigating the influence of heteroatom X within the chromophoric moiety on the reversible photoswitching process, the design of molecule **2** was implemented.

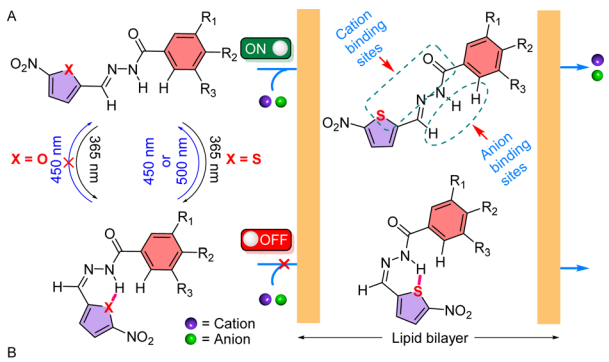

Compound	R_1	R_2	R_3	X	logP
1a	CF_3	H	CF_3	O	3.81
1b	H	CF_3	H	O	2.93
1c	H	F	H	O	2.20
2	CF_3	H	CF_3	S	4.74

Fig. 1 Chemical structure of compounds **1a–1c** and **2** with photoisomerization property and its effect on the ion transport process (A); structural description and log *P* values of designed molecules **1a–1c** and **2** (B).

2 Results and discussion

2.1 Design and synthesis of 1a–1c and 2

Acylhydrazones are known to bind to cations and anions.[50] Here, we designed an acylhydrazone-based molecule that has both cation and anion binding sites in itself. An electron withdrawing nitro group was introduced on the chromophoric moiety to reduce the double bond character of the hydrazone bond by enhancing the extended conjugation, which leads to a rapid photoswitching property. Compounds **1a–1c**, and **2** have been synthesized by following Scheme 1. Initially, compounds **3a–3c** were reacted with hydrazine monohydrate ($NH_2NH_2 \cdot H_2O$) in methanol solvent under reflux conditions to get compounds **4a–4c**. Without further purification of **4a–4c**, it was coupled separately either with 5-nitrofuran-2-carbaldehyde or 5-nitrothiophene-2-carbaldehyde in 2 : 5 water : ethanol mixture at 100 °C to get compounds **1a–1c** and **2**. All compounds are characterized with the help of ^1H, ^{13}C, HRMS, and IR data.

2.2 Photoswitching studies in UV

Initially, the photoswitching efficiency of both compounds **1a** and **2** were analyzed through UV-Vis spectroscopy in methanol solvent. Photoirradiation on compound **1a** with 365 nm of UV light for 5.5 min showed a significant bathochromic shift of the absorbance peak at 450 nm (Fig. S1A†), indicating the $E \rightarrow Z$ photoisomerization process. To validate the reversibility of the photoswitching process, the isomerized *Z*-conformer was further irradiated with 450 nm of LED light. Data revealed that even after 20 min of photoirradiation, reverse isomerization was unfeasible (Fig. S1B†).

Notably, the photoswitching study for compound **2** in methanol revealed a very rapid $E \rightarrow Z$ photoisomerization within 5 s of 365 nm irradiation (Fig. 2A and S3A†). Further, to substantiate the photo reversibility of compound **2**, an isomerized *Z*-conformer was irradiated with 450 nm light. Remarkably, after 9 min of photoirradiation, the *Z*-conformer reverts to its initial *E*-conformer (Fig. 2A and S3B†), which validated the photo reversibility of compound **2**. The

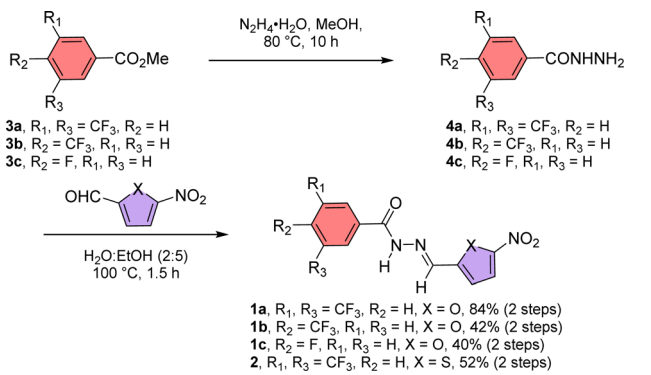

Scheme 1 Synthetic scheme of compounds **1a–1c** and **2**.

© 2024 The Author(s). Published by the Royal Society of Chemistry

Open Access Article. Published on 30 August 2024. Downloaded on 12/13/2025 10:22:42 AM. This article is licensed under a Creative Commons Attribution-NonCommercial 3.0 Unported Licence.

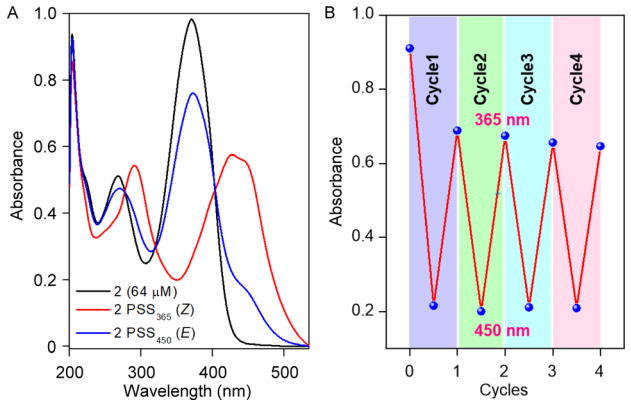

Fig. 2 UV-Vis spectrum of compound **2** showing photostationary states for 365 nm and 450 nm (A); change in absorbance value at 365 nm after each cycle of irradiation (B).

photoisomerization between *E* and *Z*-conformer was repeated for four cycles, and no major degradation was observed (Fig. 2B), which revealed that our acylhydrazone-based molecular switch remains stable even after higher photoirradiation cycles. After subjecting compound **2** to photoirradiation at both 365 nm and 450 nm, an insignificant change in the high-resolution mass spectra (HRMS) spectra was observed (Fig. S6†). Notably, the accurate molecular ion peak mass of compound **2** remained constant, indicating an efficient and reversible photoswitching process without any apparent photodegradation of the compound. Further, the presence of the UV-absorbance peak of $\mathbf{2}_Z$ conformer in 500 nm wavelength influenced us to investigate the $Z \rightarrow E$ photoisomerization with 500 nm of LED light. Efficient photoisomerization of the $\mathbf{2}_Z \rightarrow \mathbf{2}_E$ conformer was noticed upon photoirradiation with 500 nm of light for 14 min (Fig. S7†), indicating the $Z \rightarrow E$ photoisomerization can be achieved even with 500 nm of LED light. The stability of compound **2** was investigated by subjecting it to sequential photoirradiation cycles with 365 nm and 500 nm light in MeOH solvent, aiming to assess its photo reversibility (Fig. S8†). No photodegradation was observed even after four cycles, validating compound **2** can be used as a reversible efficient photoswitching system even with longer wavelength of light. The calculated photostationary state (PSS) composition during $E \rightarrow Z$ isomerization with 365 nm is $\mathbf{2}_E : \mathbf{2}_Z = 20 : 80$. Whereas the calculated PSS composition during $Z \rightarrow E$ isomerization with 450 nm and 500 nm lights is $\mathbf{2}_E : \mathbf{2}_Z = 82 : 18$ and 91 : 9, respectively.

To scrutinize the stability of the *Z*-conformer, time-dependent ^{1}H NMR was recorded in MeOH-d_4 (Fig. S9†) and MeOH-d_4 : D_2O (2 : 1 v/v) solvent (Fig. S10†) systems. Interestingly, a significant enhancement in the stability of $\mathbf{2}_Z$ conformer was noticed in the MeOH-d_4 : D_2O solvent ($\approx$48 h) compared to the MeOH-d_4 solvent ($\approx$24 h), validating the solvent-dependent thermal stability of the *Z*-conformer (Fig. S11†). The calculated photostationary state (PSS) of $\mathbf{2}_Z \rightarrow \mathbf{2}_E$ thermal relaxation is approximately 80% and 85% in MeOH-d_4 and MeOH-d_4 : D_2O solvent stems.

2.3 Ion binding studies

Ion binding efficiency of **1a–1c** and **2** were investigated by ^{1}H NMR titration in acetonitrile–d_3 with a host concentration of 2 mM.[47] Increasing the equivalent of the tetrabutylammonium chloride (TBACl) salt demonstrated a significant downfield shift of the H_a, H_b, and H_c protons, validating the involvement of these three protons in the overall ion binding process by N–H$\cdots X^-$ and two C–H$\cdots X^-$ hydrogen bonding interactions. BindFit v0.5 program[51] was further used to investigate the binding constant of compounds **1a–1c** and **2** with TBACl salt. A 1 : 1 model of host : guest confirmed that ion binding constants of **1a**, **1b**, **1c**, and **2** with TBACl salt are 995 $\pm$ 5% M^{-1}, 662 $\pm$ 6% M^{-1}, 429 $\pm$ 0.7% M^{-1}, and 935 $\pm$ 3% M^{-1} respectively (Fig. S13–S20†). The photo reversibility nature of compound **2** influenced us to investigate the ion binding process with the tetrabutylammonium halide (TBAX, $X^- = Br^-$ and I^-) salts. A 1 : 1 model of host : guest confirmed compound **2** has higher binding constants for TBACl (935 $\pm$ 3% M^{-1}), followed by TBABr (91 $\pm$ 3% M^{-1}). In contrast, the binding constant for TBAI could not be determined due to the insignificant change in the chemical shift with the sequential addition of the TBAI salt (Fig. S23†). To scrutinize the involvement of the cation in the binding process, ^{1}H NMR titration was carried out with compound **2**, titrating with $NaPF_6$ (Fig. S24†). Being a larger anion, PF_6^- is unlikely to fit in the anion binding sites, and hence, changes shown during the ^{1}H NMR titration will be due to the binding of Na^+ cation. During the NMR titration H_a, H_b, and H_c peaks are getting upfield shifted with an increase in the equivalent of $NaPF_6$ salt, indicating the Na^+ is binding to the respective cation binding sites of compound **2**. Further, ^{1}H NMR titration of compound **2** with Na^+Cl^- ion pair was investigated by mixing an equimolar amount of $NaPF_6$ and TBACl salt (Fig. S25†). Interestingly, during ion pair titration, all of the H_a, H_b, and H_c protons shift towards the downfield region with an increase in the equivalence of the guest. This data indicated compound **2** has the potential to bind both Na^+ and Cl^- ions in their respective ion binding sites. A 1 : 1 host : guest binding model by using the BindFit v0.5 program, revealed the binding constant 307 $\pm$ 14% M^{-1} (Fig. S26†).

2.4 Transmembrane ion transport activities of 1a–1c and 2

The rapid, reversible photoswitching process and significant difference in the binding constant with different salts influenced us to scrutinize the ion transport comparisons of the series of compounds **1a–1c** and **2**. An egg yolk phosphatidylcholine large unilamellar vesicles (EYPC–LUVs), entrapped with a pH-sensitive 8-hydroxypyrene-1,3,6-trisulfonate (HPTS, pK_a = 7.2) dye was used to investigate the ion transport activity of compounds **1a–1c** and **2**. Initially, a 0.8 unit of pH gradient ($pH_{in} = 7$ and $pH_{out} = 7.8$) was generated upon the addition of 20 μL of 0.5 M NaOH solution at $t = 20$ s. A change in the fluorescence intensity was monitored ($\lambda_{em} = 510$ nm, $\lambda_{ex} = 450$ nm) after the addition of the compounds **1a–1c**, and **2** separately. Finally, Titron X–100 was added ($t = 300$ s) to disintegrate the pH gradient by lysing the vesicles to achieve the complete leakage of HPTS dye.[19,52] Ion transport efficiency of compounds

Open Access Article. Published on 30 August 2024. Downloaded on 12/13/2025 10:22:42 AM. This article is licensed under a Creative Commons Attribution-NonCommercial 3.0 Unported Licence.

1a–1c, and **2** were investigated at 300 nM concentration with extravesicular and intravesicular NaCl salt. Comparison data divulge the activity sequence of **1a** > **2** > **1b** > **1c** (Fig. 3A). As expected, compounds **1a** and **2** showed higher transport efficiency among the congeners due to their optimum log *P* value (Fig. 1B), which enhanced the to-and-fro movement efficiency of the transporter molecule across the bilayer. HPTS assay was further utilized to investigate the dose-dependent studies of compounds **1a–1c**, and **2**. Half-maximal effective concentration (EC_{50}) and Hill coefficient (n) values for each analog of compounds were analyzed by the Hill equation. Hill analysis provided the $n = 2$ for all of the compounds, indicating that two monomeric units of the transporter molecule are actively involved in the overall transport process. Calculation of the EC_{50} values demonstrated that compound **1a** has the lowest EC_{50} value (71.9 nM ± 2.28, 0.106 mol%) followed by compounds **2** (365 nM ± 17.5, 0.539 mol%), **1b** (0.54 μM ± 0.05, 0.798 mol%) and **1c** (6.36 μM ± 0.39, 9.40 mol%), which also validate the transport comparison data of the compounds.

2.5 Ion selectivity studies

Irrespective of the highest ion transport activity of compound **1a**, further ion transport studies were performed with compound **2** because of its unique reversible photoswitching nature. To elucidate the involvement of different ions in the transport process, an ion selectivity assay was performed across the EYPC–LUVs ⊃ HPTS. Firstly, the anion selectivity of compound **2** by changing the extravesicular NaX ($X^- = F^-$, Cl^-, Br^-, I^-, NO_3^-, and SCN^-) salts was investigated.[52,53] A considerable change in transport activity confirmed the involvement of the anions in the transport process with a selectivity order $Cl^- > NO_3^- > F^- \approx Br^- \approx I^- > SCN^-$ (Fig. 4A). The observed anion selectivity does not follow any of the Hofmeister series,[54,55] indicating anion selectivity is controlled by both the hydration energy and the size of the anions (Fig. S33A and B†). Likewise, the involvement of the cations in the overall ion transport process was also checked by varying the extravesicular MCl salts ($M^+ = Li^+$, Na^+, K^+, Rb^+, and Cs^+).[52,53] A conspicuous change in the fluorescence activity upon variation of the extravesicular MCl salt indicated the cation selectivity with an

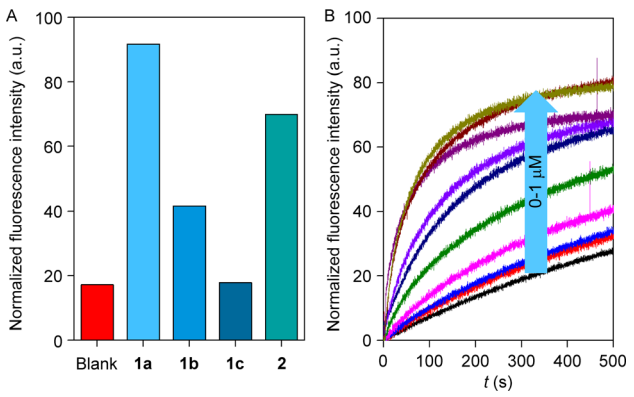

Fig. 3 Comparison of ion transport activity of **1a–1c** and **2** (A); dose–response study of **2** across EYPC–LUVs ⊃ HPTS (B).

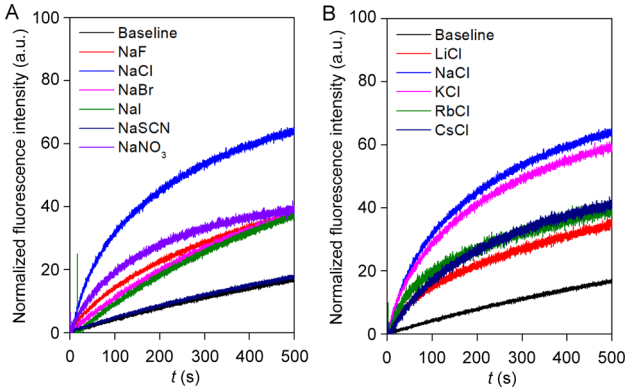

Fig. 4 Ion selectivity of compound **2** across EYPC–LUVs ⊃ HPTS towards anion (A); and cation (B) at 300 nM concentration.

activity sequence $Na^+ > K^+ > Rb^+ \approx Cs^+ > Li^+$ (Fig. 4B). The observed cation selectivity suggested that both the size and hydration energy of the cation regulate the overall cation selectivity (Fig. S33C and D†).[54,56] Further, ^{23}Na NMR was utilized for the confirmation of the cation transport property of compound **2**. A shift reagent was added externally to distinguish the external and internal Na^+ signals. The change in the extravesicular Na^+ signal was monitored by increasing the concentration of compound **2**. A prominent change in the Na^+ ion transport rate was observed with increasing the concentration of compound **2** (Fig. S37†), indicating that compound **2** is capable of transporting Na^+ ions across the bilayer membrane. Hence, the aforementioned selectivity studies divulge the involvement of both cation and anion in the overall transport process.

2.6 Chloride influx and cation selectivity studies

To ensure the chloride transport activity of compound **2**, a halide-sensitive lucigenin dye,[57] 200 mM $NaNO_3$ salt with pH = 7.0, was encapsulated in EYPC–LUVs. A Cl^-/NO_3^- gradient was created by the addition of 33.3 μL from 2 M NaCl salt in the extravesicular medium, and the change in the fluorescence activity was monitored at $\lambda_{em} = 535$ nm ($\lambda_{ex} = 455$ nm) with time. At $t = 300$ s, Titron-X 100 was added to lyse the vesicles.[57,58] The increasing concentration of the compound gradually increased the fluorescence quenching of the lucigenin dye, demonstrating the chloride influxing capability of compound **2** (Fig. S35†). Hill analysis provided the EC_{50} value 2.47 μM ± 0.18 and the Hill coefficient $n = 2$, reiterating the aforementioned Hill coefficient values of our transporters during the HPTS assay.

The cation selectivity of compound **2** was further reconfirmed across the EYPC–LUVs ⊃ lucigenin. A chloride gradient was created by the addition of 33.3 μL of 2 M MCl salts ($M^+ = Li^+$, Na^+, K^+, Rb^+, and Cs^+) in the extravesicular medium at $t = 20$ s. A change in the fluorescence quenching activity of lucigenin was monitored after the addition of compound **2** at $t = 100$ s. Variation in the extravesicular cations conspicuously changed the lucigenin fluorescence quenching activity (Fig. S36†), demonstrating compound **2** is selective towards

© 2024 The Author(s). Published by the Royal Society of Chemistry

Open Access Article. Published on 30 August 2024. Downloaded on 12/13/2025 10:22:42 AM. This article is licensed under a Creative Commons Attribution-NonCommercial 3.0 Unported Licence.

cations with selectivity order $Na^+ > K^+ > Rb^+ > Cs^+ \approx Li^+$. The obtained cation selectivity sequence coordinates with the selectivity pattern observed during the HPTS assay.

2.7 Mechanistic studies

Increment of the HPTS fluorescence activity in the presence of the transporter molecule can be due to either antiport (OH^-/A^- or H^+/M^+ where A^- and M^+ are anions and cations) or symport (M^+/OH^-, M^+/A^- or H^+/A^-) of ions. To evaluate the operated mechanism by our transporter molecule, different experiments were conducted with compound **2**. Initially, the change in the chloride influx across the EYPC–LUVs ⊃ lucigenin was investigated in the presence of valinomycin.[59] The analogous chloride influx by compound **2** in the absence and presence of valinomycin confirmed the non-cooperative effect between compound **2** and valinomycin (Fig. S38†). The non-cooperative effect preliminary demonstrated that the compound **2** transports both cations and anions *via* the symport process. For the confirmation of the mechanistic insight into the transport process, we chose NO_3^-/SO_4^{2-} assay.[33] Here, 200 mM NaCl salt was encapsulated in the EYPC–LUVs with 1 mM lucigenin, and the pH was adjusted to 7.0. An extravesicular solution of iso-osmolar $NaNO_3$ or Na_2SO_4 was used to create the ionic gradient, and fluorescence intensity was monitored after the addition of compound **2**. SO_4^{2-} is a doubly negatively charged anion, and hence, it is difficult to transport across the bilayer as compared to the NO_3^- ion. It is expected that if compound **2** follows the antiport process as the transport mechanism, then changing the extravesicular ion from NO_3^- to SO_4^{2-} will significantly reduce the fluorescence activity gaining of the lucigenin dye. Irrespective of the extravesicular salt medium, an insignificant difference in ion transport activity for both of the extravesicular salts (Fig. S40†) was observed. This data demonstrated compound **2** can transport ions *via* a symport mechanism. Further reconfirmation of the transport mechanism was investigated by entrapping the 1 mM lucigenin dye with either iso-osmolar $NaNO_3$ salt or Na_2SO_4 salt. The Cl^- ion influx was monitored separately by creating an ionic gradient by adding NaCl salt extravesicularly. It is expected that if compound **2** follows the symport mechanism during ion transport, then changing the intravesicular salt will not affect the Cl^- ion influx. However, if it follows the antiport as a transport mechanism, then Cl^- ion influx will be negligible in the presence of intravesicular Na_2SO_4 salt compared to $NaNO_3$ salt. As expected, irrespective of the entrapped salt, a comparable amount of Cl^- ion influx was observed by compound **2** (Fig. 5A). Whereas our earlier reported compound[60] (RAS02052, Fig. S41C†), which is known to follow the antiport mechanism during the transport process, did not show any Cl^- ion influx (compound concentration 2.5 μM) in the presence of intravesicular Na_2SO_4 salt. Therefore, it is evident that compound **2** transports cation and anion by following the symport mechanism during the transport process.

The U-tube experiment was carried out to establish the mode of the ion transport (carrier or channel) by compound **2**.[61] During the experiment, the source arm (500 mM NaCl, 5 mM phosphate buffer, pH = 7.0) and the receiver arm (5 mM phosphate buffer, pH = 7.0) were separated by a 15 mL chloroform layer dissolved with 1 mM compound **2**. The practicability of a supramolecular channel to span the chloroform layer is very unlikely, and hence, it will not increase the Na^+ and Cl^- concentration in the receiver arm, but a carrier can easily shuttle across the chloroform layer and transport the Na^+ and Cl^- ion from the source arm to the receiver arm. The experimental result showed a gradual increase in the Na^+ and Cl^- concentration in the receiver arm (Fig. 5B), indicating that compound **2** follows the carrier mode of ion transport. Subsequently, ANTS–DPX assays were performed to elucidate the occurrence of large pore formation and assess membrane stability in the presence of compound **2**.[60] The experimental data revealed an indiscernible leakage of ANTS dye across the bilayer membrane in the presence of compound **2** (Fig. S42†). These findings suggest that compound **2** does not induce the formation of large pores within the bilayer and does not compromise membrane integrity.

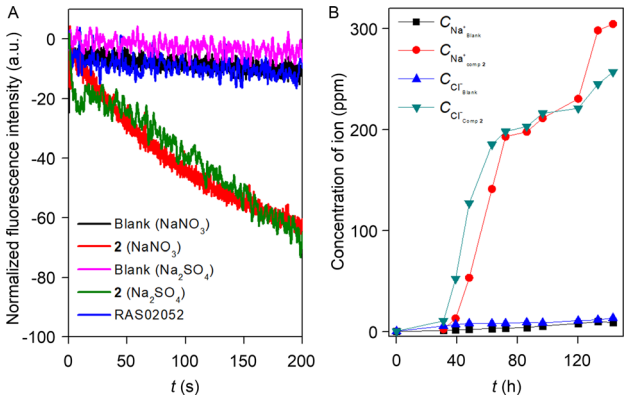

Fig. 5 Chloride influx by compound **2** (2.5 μM) across EYPC–LUVs ⊃ lucigenin with entrapped iso-osmolar $NaNO_3$ and Na_2SO_4 salt in the presence of externally added NaCl ionic pulse (A). U-tube experiment of effective NaCl symport by compound **2** by carrier mechanism (B).

2.8 Effect of photoswitching in ion transport

The effect of photoirradiation in the transport process was initially investigated across EYPC–LUVs ⊃ HPTS by irradiating the membrane-embedded compound **2** with 365 nm of light at different concentrations. It was evident from the experiment that $\mathbf{2}_E$ shows significant transport activity, whereas irradiation with 365 nm of light diminished the ion transport activity due to the $\mathbf{2}_E \rightarrow \mathbf{2}_Z$ isomerization (Fig. S44A†). A dose–response study of photoisomerized $\mathbf{2}_Z$ indicated that even at high concentrations, it remains inefficient in transporting ions (Fig. S44B†). The presence of higher absorbance intensity at 450 nm and shorter photoswitching time influenced us to scrutinize the impact of photo reversibility on the ion transport process using 450 nm light instead of 500 nm. To investigate the effect of the cation transport during the photoswitching process, a ^{23}Na NMR experiment was carried out with compound **2**. 200 mM NaCl salt encapsulated EYPC–LUVs was used during the experiment. A shift regent was added externally during the

Open Access Article. Published on 30 August 2024. Downloaded on 12/13/2025 10:22:42 AM. This article is licensed under a Creative Commons Attribution-NonCommercial 3.0 Unported Licence.

experiment to differentiate the internal and external Na^+ ion peaks. Initially, sodium ion concentrations in intravesicular and extravesicular medium are equal in equilibrium. The addition of 0.2 M sodium tri(poly)phosphate and 0.1 M dysprosium trichloride solution in 2 : 1 ratio will form Na_7-$Dy(P_3O_{10})_2 \cdot 3NaCl$. Noticeably, the addition of membrane-impermeable $Dy(P_3O_{10})^{7-}$ in the extravesicular medium makes ionic concentration unequal across the vesicular membrane. Since the large complex cannot be transported inside the vesicles through the transporter, diffusion of sodium ions through transporter **2** can be visualized by the line broadening observed for the Na^+ resonances due to the exchange of the internal and external Na^+ ions. Ion transport can be visualized and quantified by the line broadening observed for the Na^+ resonances. The exchange rate of the internal and external Na^+ ions is directly proportional to the line broadening observed for the Na^+ signal. A change in the line width of the external Na^+ ion peak was monitored during the photoirradiation of compound **2** with 365 nm and 450 nm of light prior to the addition into vesicles. As expected, a conspicuous decrement in the Na^+ transport rate was observed upon photoirradiation with 365 nm light due to the $E \rightarrow Z$ isomerization. Conversely, compound **2** achieved an initially comparable Na^+ transport rate (Fig. 6A) upon photoisomerization of $Z \rightarrow E$ conformer during exposure to 450 nm of light, demonstrating its stimulus-responsive OFF–ON transport behavior. Further, the effect of photoswitching on the chloride ion transport process was investigated through an ion-selective electrode (ISE) assay. EYPC–LUVs were entrapped with 500 mM NaCl and 10 mM sodium phosphate buffer with pH = 7.0. During the experiment, vesicles were immersed in 500 mM $NaNO_3$ and 10 mM sodium phosphate buffer with pH = 7.0 to create an ionic gradient. A stock solution compound **2** was sequentially irradiated with 365 nm and 450 nm of light and added at 50 s, and the efflux of the chloride ion was monitored by the chloride selective electrode.[47] Experimental data revealed that the *E*-conformer showed significant ion transport activity, but irradiation with 365 nm of light decreased the transport activity due to the closing of the ion binding site in the *Z*-conformer. To further understand the effect of the reversibility of $Z \rightarrow E$ conformer in the ion transport, the isomerized *Z*-conformer was irradiated with 450 nm of light to reconvert to its initial transport active *E*-conformer. As expected, it regains its initially comparable transport activity, indicating the efficient OFF–ON state of the ion transport property. Three cycles of the photoswitching process were carried out to validate the effect of the reversibility in the ion transport process. Experimental data revealed that OFF–ON transport activity can be retained even after three cycles of photoirradiation (Fig. 6B).

2.9 Theoretical studies

The X-ray crystal structure of compound **2** showed that the molecule is planar and associated with another molecule by forming a hydrogen bond.[62] To understand the motifs that are responsible for binding both cation and anion, all possible conformers were initially analyzed by the CONFLEX 8 software program.[63,64] 1306 number of possible conformations of $[(\mathbf{2}_E)_2$ + NaCl] assembly complex was obtained in the CONFLEX 8 software program. The highest populated ten conformers (Fig. S48†), along with the dimeric *E*-conformer of compound **2** were further used to optimize by Gaussian 09 program package[65,66] using B3LYP functional and 6-311++G(d,p) basis set. The $[(\mathbf{2}_E)_2$ + NaCl] complex suggested that the transporter molecule **2** participates in the anion recognition by hydrogen bonding interactions with H_a ($H_a \cdots Cl^- = 2.167$ Å), H_b ($H_b \cdots Cl^- = 2.984$ Å), and H_c ($H_c \cdots Cl^- = 2.691$ Å) protons. Whereas sodium ion binds through the electrostatic interaction between sodium cation and CONH group $C{=}O \cdots Na^+$ (2.283 Å), hydrazone nitrogen atom $N \cdots Na^+$ (2.643 Å) and sulfur atom $S \cdots Na^+$ (2.870 Å) (Fig. 7A). The binding energy of the geometrically optimized $[(\mathbf{2}_E)_2$ + NaCl] complex was calculated to be −28.22 kcal mol^{-1} (Table S3†).

Further, to unveil the reason for reversibility in the photoswitching of compound **2**, the highest populated two conformers of compounds $\mathbf{1a}_Z$ and $\mathbf{2}_Z$ were geometrically optimized by the Gaussian 09 program with B3LYP functional and 6-311++G(d,p) basis set after analyzing all possible conformers with CONFLEX 8 software program. Geometry optimization of

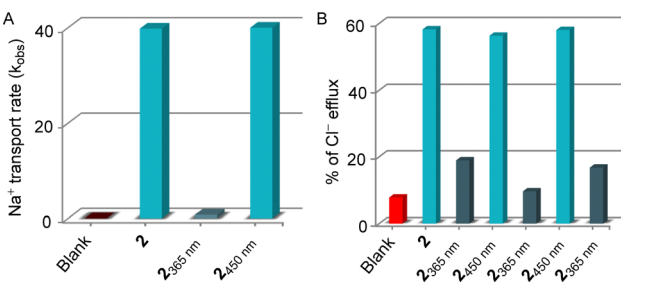

Fig. 6 ^{23}Na NMR experiment to investigate the effect of light in Na^+ transport rate by compound **2** (3.42 mol% relatives to phospholipids) across EYPC–LUVs (A); effect in Cl^- efflux by **2** (4.11 mol% relatives to phospholipids) upon repeating photoirradiation with different wavelength of light (B).

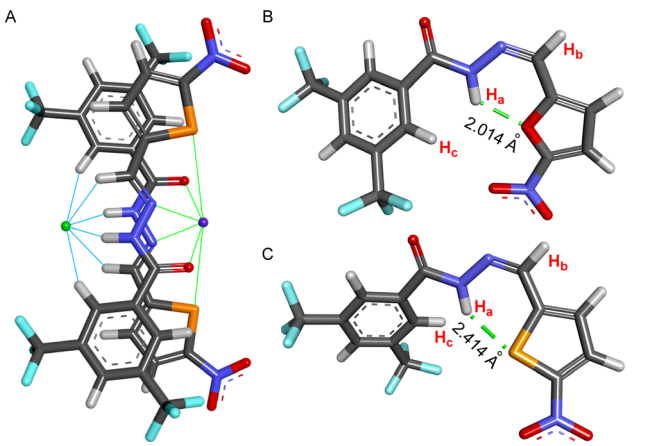

Fig. 7 Geometry optimized structure of $[(\mathbf{2}_E)_2$ + NaCl] complex with different hydrogen bonds and electrostatic interactions to bind anion and cation (A); geometry optimized structure of $\mathbf{1a}_Z$ (B), and $\mathbf{2}_Z$ with intramolecular hydrogen bond (C).

© 2024 The Author(s). Published by the Royal Society of Chemistry

Open Access Article. Published on 30 August 2024. Downloaded on 12/13/2025 10:22:42 AM. This article is licensed under a Creative Commons Attribution-NonCommercial 3.0 Unported Licence.

compounds $\mathbf{1a}_Z$ and $\mathbf{2}_Z$ suggested that the **conf-II**$_Z$ is the most stable for both of the compounds. Further, natural bond orbital (NBO) analysis[67] and the corresponding hydrogen bond interaction energies (E^2) were carried out with **conf-II**$_Z$ of $\mathbf{1a}_Z$ and $\mathbf{2}_Z$. Investigation divulged that in $\mathbf{1a}_Z$ the oxygen atom (LP 1) in the chromophoric moiety formed an intramolecular H-bond with H_a proton with an interaction energy of 3.92 kcal mol^{-1} (Fig. 7B), whereas in $\mathbf{2}_Z$ the sulfur atom (LP 1) in the chromophoric moiety formed an intramolecular H-bond with H_a proton with comparatively lesser interaction energy of 2.58 kcal mol^{-1} (Fig. 7C). Further, evidence of the formation of a stronger H-bond in the case of $\mathbf{1a}_Z$ also reflects from its shorter H-bonding distance. Lesser H-bonding strength and larger H-bonding length in $\mathbf{2}_Z$, make it a suitable candidate for reversible photoisomerization.

3 Conclusions

We introduced the first example of a reversibly photoswitched acylhydrazone-based ion transporter system that transports cations and anions across the bilayer membrane. A series of molecules were synthesized by varying the lipophilicity. Among the series, although compound **1a** showed higher transport activity, compound **2** has unique reversible photoswitching properties. Compound **2** can be reversibly photoswitched by sequential photoirradiation with 365 nm and 450 nm of light as well as 365 nm and 500 nm of light. Ion selectivity studies confirmed its higher selectivity towards Na^+ and Cl^- ions. The mechanistic study revealed that compound **2** transports ions *via* the symport mechanism by following the carrier mode of ion transport. Further, the dose–response studies in lucigenin assay demonstrated the chloride influx ability of compound **2**. The effect of the photoswitching process in ion transport revealed the OFF–ON transport of compound **2** on sequential repetitive photoirradiation with 365 nm and 450 nm of light. The mode of binding of compound **2** with NaCl as well as the reason for reversible photoisomerization of transporter **2** were finally studied using geometry optimization and natural bond orbital analysis, which strongly validates the experimental evidence. Hence, we believe these acylhydrazone-based small transporter molecules have the potential to be utilized as a photoresponsive ion transport system with reversible OFF–ON transport activity upon photoirradiation. We are certain that in the future, this can open up a new avenue for utilizing these acylhydrazone-based reversibly photoswitchable cation–anion transport systems for real-life biological applications.

Data availability

Crystallographic data for compound **2** has been deposited at the Cambridge Crystallographic Data Centre (CCDC) under deposition number 2340801.[62] The datasets supporting this article have been uploaded as part of the ESI.† Data for this paper, including synthesis, compound characterization, experimental procedures, and theoretical calculations, are available in the ESI.†

Author contributions

P. T. conceived the project and directed the experimental studies. P. W. synthesized and characterized the compounds and investigated the ion binding studies. S. C. performed the ion transport studies and the computational studies. S. C. and P. T. wrote the manuscript. All authors approved the final version of the manuscript.

Conflicts of interest

There are no conflicts to declare.

Acknowledgements

PT acknowledges the support of the Science and Engineering Research Board, Govt. of India (Project No. CRG/2022/001640) and IISER Pune. SC thanks the Prime Minister Research Fellowship (PMRF), Government of India, for research fellowships. We acknowledge the computational support and the resources provided by 'PARAM Brahma Facility' under the National Supercomputing Mission, Government of India at IISER, Pune. We also thank Mr Sourav Mandal for his help during the theoretical calculation.

Notes and references

1 L. Song, M. R. Hobaugh, C. Shustak, S. Cheley, H. Bayley and J. E. Gouauxt, *Science*, 1996, **274**, 1859–1866.
2 T. E. DeCoursey, K. G. Chandy, S. Gupta and M. D. Cahalan, *Nature*, 1984, **307**, 465–468.
3 S. Y. Chiu and G. F. Wilson, *J. Physiol.*, 1989, **408**, 199–222.
4 J. M. Russell, *Physiol. Rev.*, 2000, **80**, 211–276.
5 J. A. Payne, C. Rivera, J. Voipio and K. Kaila, *Trends Neurosci.*, 2003, **26**, 199–206.
6 P. Blaesse, M. S. Airaksinen, C. Rivera and K. Kaila, *Neuron*, 2009, **61**, 820–838.
7 G. Bernard and M. I. Shevell, *Pediatr. Neurol.*, 2008, **38**, 73–85.
8 J. Y. Choi, D. Muallem, K. Kiselyov, M. G. Lee, P. J. Thomas and S. Muallem, *Nature*, 2001, **410**, 94–97.
9 T. J. Jentsch, T. Maritzen and A. A. Zdebik, *J. Clin. Invest.*, 2005, **115**, 2039–2046.
10 J.-L. Galzi, A. Devillers-Thiery, N. Hussy, S. Bertrand, J.-P. Changeux and D. Bertrand, *Nature*, 1992, **359**, 500–505.
11 W. Grosse, L.-O. Essen and U. Koert, *ChemBioChem*, 2011, **12**, 830–839.
12 S. Reitz, M. Cebi, P. Reiß, G. Studnik, U. Linne, U. Koert and L.-O. Essen, *Angew. Chem., Int. Ed.*, 2009, **48**, 4853–4857.
13 P. Xin, H. Kong, Y. Sun, L. Zhao, H. Fang, H. Zhu, TaoJiang, J. Guo, Q. Zhang, W. Dong and C.-P. Chen, *Angew. Chem., Int. Ed.*, 2019, **58**, 2779–2784.
14 W.-L. Huang, X.-D. Wang, Y.-F. Ao, Q.-Q. Wang and D.-X. Wang, *J. Am. Chem. Soc.*, 2020, **142**, 13273–13277.
15 P. A. Gale, J. T. Davis and R. Quesada, *Chem. Soc. Rev.*, 2017, **46**, 2497–2519.

Open Access Article. Published on 30 August 2024. Downloaded on 12/13/2025 10:22:42 AM. This article is licensed under a Creative Commons Attribution-NonCommercial 3.0 Unported Licence.

16 A. I. Share, K. Patel, C. Nativi, E. J. Cho, O. Francesconi, N. Busschaert, P. A. Gale, S. Roelens and J. L. Sessler, *Chem. Commun.*, 2016, **52**, 7560–7563.
17 S. Dey, A. Patel, N. Haloi, S. Srimayee, S. Paul, G. K. Barik, N. Akhtar, D. Shaw, G. Hazarika, B. M. Prusty, M. Kumar, M. K. Santra, E. Tajkhorshid, S. Bhattacharjee and D. Manna, *J. Med. Chem.*, 2023, **66**, 11078–11093.
18 M. R. Ghadlri, J. R. Granja and L. K. Buehler, *Nature*, 1994, **369**, 301–304.
19 J. A. Malla, R. M. Umesh, A. Vijay, A. Mukherjee, M. Lahiri and P. Talukdar, *Chem. Sci.*, 2020, **11**, 2420–2428.
20 S.-H. Park, S.-H. Park, E. N. W. Howe, J. Y. Hyun, L.-J. Chen, I. Hwang, G. Vargas-Zuñiga, N. Busschaert, P. A. Gale, J. L. Sessler and I. Shin, *Chem*, 2019, **5**, 2079–2098.
21 F.-F. Shen, S.-Y. Dai, N.-K. Wong, S. Deng, A. S.-T. Wong and D. Yang, *J. Am. Chem. Soc.*, 2020, **142**, 10769–10779.
22 R. Sasaki, K. Sato, K. V. Tabata, H. Noji and K. Kinbara, *J. Am. Chem. Soc.*, 2021, **143**, 1348–1355.
23 R. Ye, C. Ren, J. Shen, N. Li, F. Chen, A. Roy and H. Zeng, *J. Am. Chem. Soc.*, 2019, **141**, 9788–9792.
24 F. Zeng, F. Liu, L. Yuan, S. Zhou, J. Shen, N. Li, H. Ren and H. Zeng, *Org. Lett.*, 2019, **21**, 4826–4830.
25 P. H. Schlesinger, R. Ferdani, J. Liu, J. Pajewska, R. Pajewski, M. Saito, H. Shabany and G. W. Gokel, *J. Am. Chem. Soc.*, 2002, **124**, 1848–1849.
26 M. Merritt, M. Lanier, G. Deng and S. L. Regen, *J. Am. Chem. Soc.*, 1998, **120**, 8494–8501.
27 A. V. Koulov, J. M. Mahoney and B. D. Smith, *Org. Biomol. Chem.*, 2003, **1**, 27–29.
28 J. H. Lee, J. H. Lee, Y. R. Choi, P. Kang, M.-G. Choi and K.-S. Jeong, *J. Org. Chem.*, 2014, **79**, 6403–6409.
29 C. C. Tong, R. Quesada, J. L. Sessler and P. A. Gale, *Chem. Commun.*, 2008, 6321–6323.
30 A. V. Jentzsch, D. Emery, J. Mareda, P. Metrangolo, G. Resnati and S. Matile, *Angew. Chem., Int. Ed.*, 2011, **50**, 11675–11678.
31 Z. Zhao, B. Tang, X. Yan, X. Wu, Z. Li, P. A. Gale and Y.-B. Jiang, *Front. Chem. Sci. Eng.*, 2022, **16**, 81–91.
32 D. Basak, S. Sridhar, A. K. Bera and N. Madhavan, *Org. Biomol. Chem.*, 2016, **14**, 4712–4717.
33 S. Chattopadhayay, A. Ghosh, T. K. Mukhopadhyay, R. Sharma, A. Datta and P. Talukdar, *Angew. Chem., Int. Ed.*, 2023, **62**, e202313712.
34 L. Lien, D. C. J. Jaikaran, Z. Zhang and G. A. Woolley, *J. Am. Chem. Soc.*, 1996, **118**, 12222–12223.
35 E. N. W. Howe, N. Busschaert, X. Wu, S. N. Berry, J. Ho, M. E. Light, D. D. Czech, H. A. Klein, J. A. Kitchen and P. A. Gale, *J. Am. Chem. Soc.*, 2016, **138**, 8301–8308.
36 Y. R. Choi, B. Lee, J. Park, W. Namkung and K.-S. Jeong, *J. Am. Chem. Soc.*, 2016, **138**, 15319–15322.
37 A. Docker, T. G. Johnson, H. Kuhn, Z. Zhang and M. J. Langton, *J. Am. Chem. Soc.*, 2023, **145**, 2661–2668.
38 J. A. Malla, R. M. Umesh, S. Yousf, S. Mane, S. Sharma, M. Lahiri and P. Talukdar, *Angew. Chem., Int. Ed.*, 2020, **59**, 7944–7952.
39 P. Talukdar, B. Pinaki, M. Guillaume, S. Jiri and M. Naomi, *Chem.–Eur. J.*, 2005, **11**, 6525–6532.
40 M. R. Banghart, M. Volgraf and D. Trauner, *Biochemistry*, 2006, **45**, 15129–15141.
41 S. J. Wezenberg, L.-J. Chen, J. E. Bos, B. L. Feringa, E. N. W. Howe, X. Wu, M. A. Siegler and P. A. Gale, *J. Am. Chem. Soc.*, 2022, **144**, 331–338.
42 W.-Z. Wang, L.-B. Huang, S.-P. Zheng, E. Moulin, O. Gavat, M. Barboiu and N. Giuseppone, *J. Am. Chem. Soc.*, 2021, **143**, 15653–15660.
43 T. G. Johnson, A. Sadeghi-Kelishadi and M. J. Langton, *J. Am. Chem. Soc.*, 2022, **144**, 10455–10461.
44 T. Liu, C. Bao, H. Wang, Y. Lin, H. Jia and L. Zhu, *Chem. Commun.*, 2013, **49**, 10311–10313.
45 S. B. Salunke, J. A. Malla and P. Talukdar, *Angew. Chem., Int. Ed.*, 2019, **58**, 5354–5358.
46 L. E. Bickerton and M. J. Langton, *Chem. Sci.*, 2022, **13**, 9531–9536.
47 M. Ahmad, S. Chattopadhayay, D. Mondal, T. Vijayakanth and P. Talukdar, *Org. Lett.*, 2021, **23**, 7319–7324.
48 M. Ahmad, N. J. Roy, A. Singh, D. Mondal, A. Mondal, T. Vijayakanth, M. Lahiri and P. Talukdar, *Chem. Sci.*, 2023, **14**, 8897–8904.
49 Y. Zhou, Y. Chen, P.-P. Zhu, W. Si, J.-L. Hou and Y. Liu, *Chem. Commun.*, 2017, **53**, 3681–3684.
50 Z. Kokan and M. J. Chmielewski, *J. Am. Chem. Soc.*, 2018, **140**, 16010–16014.
51 *BindFit v0.5*, **https://www.app.supramolecular.org/bindfit/**.
52 T. Saha, A. Gautam, A. Mukherjee, M. Lahiri and P. Talukdar, *J. Am. Chem. Soc.*, 2016, **138**, 16443–16451.
53 T. Saha, M. S. Hossain, D. Saha, M. Lahiri and P. Talukdar, *J. Am. Chem. Soc.*, 2016, **138**, 7558–7567.
54 Y. Marcus, *J. Chem. Soc., Faraday Trans.*, 1991, **87**, 2995–2999.
55 E. M. Wright and J. M. Diamond, *Physiol. Rev.*, 1977, **57**, 109–156.
56 G. Eisenman and R. Horn, *J. Membr. Biol.*, 1983, **76**, 197–225.
57 J. Biwersi, B. Tulk and A. S. Verkman, *Anal. Biochem.*, 1994, **219**, 139–143.
58 B. P. Benke, P. Aich, Y. Kim, K. L. Kim, M. R. Rohman, S. Hong, I.-C. Hwang, E. H. Lee, J. H. Roh and K. Kim, *J. Am. Chem. Soc.*, 2017, **139**, 7432–7435.
59 S. V. Shinde and P. Talukdar, *Angew. Chem., Int. Ed.*, 2017, **56**, 4238–4242.
60 R. Sharma, S. Sarkar, S. Chattopadhayay, J. Mondal and P. Talukdar, *Angew. Chem., Int. Ed.*, 2024, **63**, e202319919.
61 Q. He, G. M. Peters, V. M. Lynch and J. L. Sessler, *Angew. Chem., Int. Ed.*, 2017, **56**, 13396–13400.
62 S. Chattopadhayay, P. Wanjari and P. Talukdar, CCDC 2340801: Experimental Crystal Structure Determination, 2024, DOI: **10.5517/ccdc.csd.cc2jksqm**.
63 H. Goto and E. Osawa, *J. Am. Chem. Soc.*, 1989, **111**, 8950–8951.
64 H. Goto, S. Obata, N. Nakayama and K. Ohta, *CONFLEX 8*, CONFLEX Corporation, Tokyo, Japan, 2017.
65 M. J. Frisch, J. A. Pople and J. S. Binkley, *J. Chem. Phys.*, 1984, **80**, 3265–3269.
66 M. J. Frisch, G. W. Trucks, H. B. Schlegel, G. E. Scuseria, M. A. Robb, J. R. Cheeseman, G. Scalmani, V. Barone,

© 2024 The Author(s). Published by the Royal Society of Chemistry

Open Access Article. Published on 30 August 2024. Downloaded on 12/13/2025 10:22:42 AM.
This article is licensed under a Creative Commons Attribution-NonCommercial 3.0 Unported Licence.

B. Mennucci, G. A. Petersson, H. Nakatsuji, M. Caricato, X. Li, H. P. Hratchian, A. F. Izmaylov, J. Bloino, G. Zheng, J. L. Sonnenberg, M. Hada, M. Ehara, K. Toyota, R. Fukuda, J. Hasegawa, M. Ishida, T. Nakajima, Y. Honda, O. Kitao, H. Nakai, T. Vreven, J. A. Montgomery Jr, J. E. Peralta, F. Ogliaro, M. Bearpark, J. J. Heyd, E. Brothers, K. N. Kudin, V. N. Staroverov, T. Keith, R. Kobayashi, J. Normand, K. Raghavachari, A. Rendell, J. C. Burant, S. S. Iyengar, J. Tomasi, M. Cossi, N. Rega, J. M. Millam, M. Klene, J. E. Knox, J. B. Cross, V. Bakken, C. Adamo, J. Jaramillo, R. Gomperts, R. E. Stratmann, O. Yazyev, A. J. Austin, R. Cammi, C. Pomelli, J. W. Ochterski, R. L. Martin, K. Morokuma, V. G. Zakrzewski, G. A. Voth, P. Salvador, J. J. Dannenberg, S. Dapprich, A. D. Daniels, O. Farkas, J. B. Foresman, J. V. Ortiz, J. Cioslowski and D. J. Fox, *Gaussian 09, Rev. D.01*, Gaussian, Inc., Wallingford, CT, 2013.

67 E. D. Glendening, C. R. Landis and F. Weinhold, *J. Comput. Chem.*, 2013, **34**, 1429–1437.